JGR Space Physics

RESEARCH ARTICLE
10.1029/2019JA027641

Key Points:
- The pattern of latitudinal distribution of irregularities is investigated in the African region
- The distribution shows hemispheric asymmetry in terms of latitudinal boundary
- The 17 March 2015 storm event inhibited the appearance of irregularities for the storm days considered

Pattern of Latitudinal Distribution of Ionospheric Irregularities in the African Region and the Effect of March 2015 St. Patrick's Day Storm

O. S. Bolaji[1,2], S. J. Adebiyi[3], J. B. Fashae[1,4], S. O. Ikubanni[3], H. A. Adenle[1], and C. Owolabi[5]

[1]Department of Physics, University of Lagos, Lagos, Nigeria, [2]Department of Physics, University of Tasmania, Hobart, Tasmania, Australia, [3]Department of Physics, Space Weather group, Landmark University, Omu-Aran, Nigeria, [4]Department of Physics, Bowen University, Iwo, Nigeria, [5]Department of Geophysics and Planetary Science, University of Science and Technology of China, Hefei, China

Correspondence to:
S. J. Adebiyi,
johndat2003@gmail.com;
adebiyi.shola@lmu.edu.ng

Citation:
Bolaji, O. S., Adebiyi, S. J., Fashae, J. B., Ikubanni, S. O., Adenle, H. A., & Owolabi, C. (2020). Pattern of latitudinal distribution of ionospheric irregularities in the African region and the effect of March 2015 St. Patrick's Day storm. *Journal of Geophysical Research: Space Physics*, *125*, e2019JA027641. https://doi.org/10.1029/2019JA027641

Received 14 NOV 2019
Accepted 18 JAN 2020
Accepted article online 6 FEB 2020

Abstract This paper investigates the latitudinal distribution of quiet and storm time irregularities over the African ionosphere in the month of March 2015. The average rate of change in total electron content (TEC) index ($ROTI_{ave}$) calculated from Global Positioning System data is used as a proxy for the irregularities. The result during the quiet condition shows that irregularities are mostly observed between 19:00 and 00:00 LT regardless of the hemisphere. Its appearance in the Southern Hemisphere is earlier, though with less severity mainly around the equatorward edge of the equatorial anomaly peak. The peak of its development occurred at 21:00 LT, as it is observed in all the latitudes except those outside the equatorial region. The strength is found to be most severe at ~12° magnetic latitude (up to 1.10 TECU/min.) in the south. Beyond ~18° magnetic latitude, it is rarely noticed in the south. However, it is not observed around this latitude in the north, indicating a major hemispheric asymmetry in terms of the latitudinal boundary between the Northern and Southern Hemispheres. Furthermore, its disappearance is found to be most rapid around the poleward verge of the equatorial anomaly region particularly in the Southern Hemisphere. In contrast to quiet time observations, irregularities were absent in all latitudes during the storm days considered. This can be attributed to the local time of the storm's onset and the possible imposition of westward electric fields in the dusk period.

1. Introduction

The appearance of irregularities in the ionosphere due to its variability may pose a serious threat to radio waves propagating through it. The interaction between radio signals and irregular ionospheric plasma structure may lead to a rapid fluctuation in the phase and amplitude of the signals, which are called phase and amplitude scintillations, respectively. Ionospheric scintillation can cause significant degradation in signals quality (i.e., reduction of the information content of the signals), communication/navigation errors, and if the scintillation is sufficiently intense, it could lead to complete navigational failure (Kintner et al., 2007).

Previous investigations have shown that ionospheric scintillation is more typical at the equatorial and low-latitude region soon after the local sunset (Mungufeni et al., 2016; Ngwira et al., 2013). Ionospheric scintillations are caused when radio signals propagate through an inhomogeneous ionosphere. The cause of the inhomogeneity in the *F* region ionospheric structure at the equatorial region has been linked to a series of multistep plasma processes involving interchange of plasma Rayleigh-Taylor (R-T) and E × B instabilities operating at the *F*2 region immediately after the sunset (Fejer et al., 1999). The R-T instability occurs in the ionosphere when light plasma (due to plasma depletion associated with the absence of solar radiation at that period) at the bottom of the *F*2 layer is accelerated into dense plasma. The R-T instability is triggered by postsunset enhancement of eastward electric field (De Rezende et al., 2007). It is well known that enhancement in the eastward electric field at the equatorial region immediately after the sunset is the cause of the upward motion of plasma around that period (known as prereversal velocity enhancement). Investigations by Anderson et al. (2004), Li et al. (2008), and Kil et al. (2009) have reported that the main contributor to the development of postsunset equatorial ionospheric irregularities is the size of the

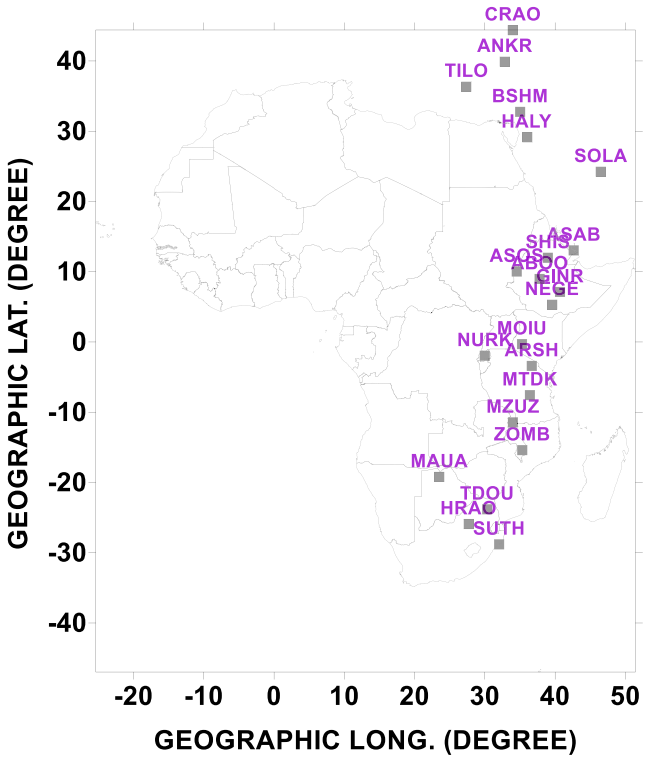

Figure 1. Plot showing the geographic locations of the GPS receivers used for the investigation.

prereversal vertical plasma drift of electron density and is associated with the intensification of the eastward electric field around the postsunset periods.

Studies of ionospheric irregularities have been a subject of extensive investigation over several decades. These studies have revealed the dependence of ionospheric irregularities on local time, season, longitude, latitude solar, and magnetic activities (Mungufeni et al., 2016; Bolaji et al., 2019; Amaechi et al., 2018; Dugassa et al., 2019; Muella et al., 2008; Ngwira et al., 2013; Oladipo & Schüler, 2013a, 2013b). The ionosphere in the African region, which has the history of been less investigated compared to other sectors, has been reported by Kintner et al. (2009) to show more severe effects on transionospheric signals. Furthermore, most studies involving irregularities in the African ionosphere have mainly focused on its variability at individual stations (e.g., Oladipo and Schüler, 2013a; Olwendo et al., 2013; Wiens et al., 2006) or using a few number of stations to investigate its longitudinal dependence during different geomagnetic conditions (e.g., Mungufeni et al., 2016; Ngwira et al., 2013). For example, the seasonal dependence of the occurrence of Equatorial Plasma Bubbles over Asmara, Eritrea, in East Africa, has been investigated by Wiens et al. (2006). The seasonal variation of ionospheric scintillation over Nairobi, Kenya, was also investigated by Olwendo et al. (2013). Recently, Mungufeni et al. (2016) investigated the solar activity pattern of irregularities using four different stations spanning from east to west in African region. However, studies on the pattern of latitudinal distribution of irregularities have not yet been fully investigated over the region. Simultaneous investigation over the entire latitudes in both hemispheres may provide insight to less known features in the region. Such investigation may provide information which may include the frequency, the latitudinal boundaries, and the severity in the distribution pattern of irregularities.

Consequently, this paper is aimed at investigating the latitudinal distribution of irregularities in the African region during quiet and storm periods. Global Positioning System (GPS) data for the month of March 2015 were used for the investigation. The GPS data were those from receivers located within the 23–40°E meridians and spanning through the entire latitudes in the region. The distribution during the 17 March 2015 major geomagnetic disturbance was also investigated.

2. Data and Method of Analysis

In this paper, the average rate of change of TEC index (ROTI) derived from the GPS data is used as a proxy to indicate the fluctuation level due to the presence of irregularities. The Receiver INdependent EXchange files that are largely available from the databases of International Global Navigation Satellite System (GNSS) Service (ftp://garner.ucsd.edu/rinex/) and African Geodetic Reference Frame (AFREF) (http://www.afref-data.org) were used. The International GNSS Service is a collection of over 300 permanent ground-based heterogeneous GNSS receivers that collect, archive, and distribute GNSS data products. The AFREF project is primarily designed to unify all the GNSS networks in Africa including those from the national mapping agencies and universities. Thus, measurements from the GPS receivers within the longitudes 23–40°E and spanning from the dip equator down to the low latitudes in both hemispheres were used. Figure 1 shows the distributions of these receivers, while Table 1 indicates the geophysical information of those locations. The GPS data are collected for the month of March 2015 and are processed using the GPS-Global Navigation Satellite System (GNSS) analysis application developed at the Institute of Scientific Research, Boston College, USA.

Many authors have used different indices as a proxy for irregularities in the ionosphere. For example, Mendillo et al. (2000) and Lee et al. (2009) employed F_P index, Li et al. (2007) used power spectral index (n), while Pi et al. (1997), Oladipo and Schüler (2013a, 2013ab), Li et al. (2010), and Deng et al. (2014)

Table 1
The List of the Stations Used and Their Corresponding Geographic and Geomagnetic Coordinates

S/N	Location	Country	Station Code	Geographic		Geomagnetic		Local Time
				Lat.	Long.	Lat.	Long.	
1	Sutherland	South Africa	SUTH	−28.78	32.03	−38.57	102.82	UT + 2 hr
2	Krugersdorp	South Africa	HRAO	−25.89	27.68	−36.31	94.61	UT + 2 hr
3	Thohoyandou	South Africa	TDOU	−23.79	30.33	−34.10	98.37	UT + 2 hr
4	Maua	Botswana	MAUA	−19.19	23.52	−30.12	92.51	UT + 2 hr
5	Zomba	Malawi	ZOMB	−15.37	35.32	−26.06	105.58	UT + 2 hr
6	Mzuz	Malawi	MZUZ	−11.42	34.00	−21.87	104.91	UT + 2 hr
7	Mtandika	Tanzania	MTDK	−7.54	36.42	−17.56	107.79	UT + 2 hr
8	Arusha	Tanzania	ARSH	−3.39	36.69	−13.03	10.32	UT + 2 hr
9	Kigali	Rwanda	NURK	−1.94	30.00	−11.62	101.57	UT + 2 hr
10	Eldoret	Kenya	MOIU	−0.28	35.29	−9.18	107	UT + 2 hr
11	Negele	Ethiopia	NEGE	5.33	39.58	−3.60	11.33	UT + 3 hr
12	Ginir	Ethiopia	GINR	7.14	40.70	−1.59	112.46	UT + 3 hr
13	Aboo	Ethiopia	ABOO	8.99	37.80	0.01	109.48	UT + 3 hr
14	Assosa	Ethiopia	ASOS	10.05	34.55	0.69	106.17	UT + 2 hr
15	Shimsheba	Ethiopia	SHIS	12.00	38.98	3.28	110.62	UT + 3 hr
16	Asab	Ethiopia	ASAB	13.06	42.65	6.79	110.47	UT + 3 hr
17	Solar Village	Saudi Arabia	SOLA	24.26	46.51	17.71	118.16	UT + 3 hr
18	Halat Ammar	Saudi Arabia	HALY	29.16	36.07	21.85	107.53	UT + 2 hr
19	Haifa	Israel	BSHM	32.77	35.02	26.00	106.62	UT + 2 hr
20			TILO	36.38	27.39	29.45	99.46	UT + 2 hr
21	Ankara	Turkey	ANKR	39.93	32.85	34.29	105.06	UT + 2 hr
22	Simeiz	Ukraine	CRAO	44.41	33.99	39.48	106.71	UT + 2 hr

used rate of TEC index (ROTI) as a measure of the fluctuation level. In this paper, a 30-min average of ROTI (in TECU/min) derived from GPS observations is employed. The ROTI is a good proxy for detecting the presence of ionospheric irregularities, and it captured the GPS phase fluctuation due to plasma depletion during the postsunset periods. The ROT and hence ROTI (one of the ROT-derived parameters) are computed using equations (1) and (2), respectively:

$$\mathrm{ROT} = \frac{\mathrm{TEC}}{t} \tag{1}$$

$$\mathrm{ROTI} = \sqrt{<\mathrm{ROT}^2> - <\mathrm{ROT}>^2} \tag{2}$$

where ROT is the detrended rate of change of TEC, t is the change in time in minute, TEC is change in TEC obtained by subtracting each TEC from its previous value, and ROTI is defined as the standard deviation of ROT over a 5-min interval (Pi et al., 1997). In order to minimize the multipath effect, the estimation of ROTI is done using the TEC data from satellites with elevation angle greater than 30°. The 30-min ROTI index is estimated and used to represent the phase fluctuations level over a location. The 30-min resolution is the average value of ROTI ($\mathrm{ROTI_{ave}}$) over a 30-min period for all the satellites in view at a particular location. In this study, the presence of irregularities is indicated based on a certain $\mathrm{ROTI_{ave}}$ threshold values defined in the investigation by Oladipo and Schüler (2013a), where $\mathrm{ROTI_{ave}}$<0.4 TECU/min indicates the background irregularities (i.e., absent of irregularities), 0.4< $\mathrm{ROTI_{ave}}$ < 0.8 indicates the presence of moderate irregularities, and $\mathrm{ROTI_{ave}} > 0.8$ indicates the occurrence of severe irregularities.

3. Results and Discussions

3.1. Latitudinal Distribution of Irregularities During Quiet Condition

Figure 2 shows the variation of $\mathrm{ROTI_{ave}}$ over the entire stations in the Northern Hemisphere for all the days in the month under investigation, while Figure 3 is for stations in the Southern Hemisphere. The result obtained shows that irregularities are observed at stations from the dip equator up to around the equatorial anomaly (EA) region irrespective of the hemisphere. It was however not seen at locations beyond the EA

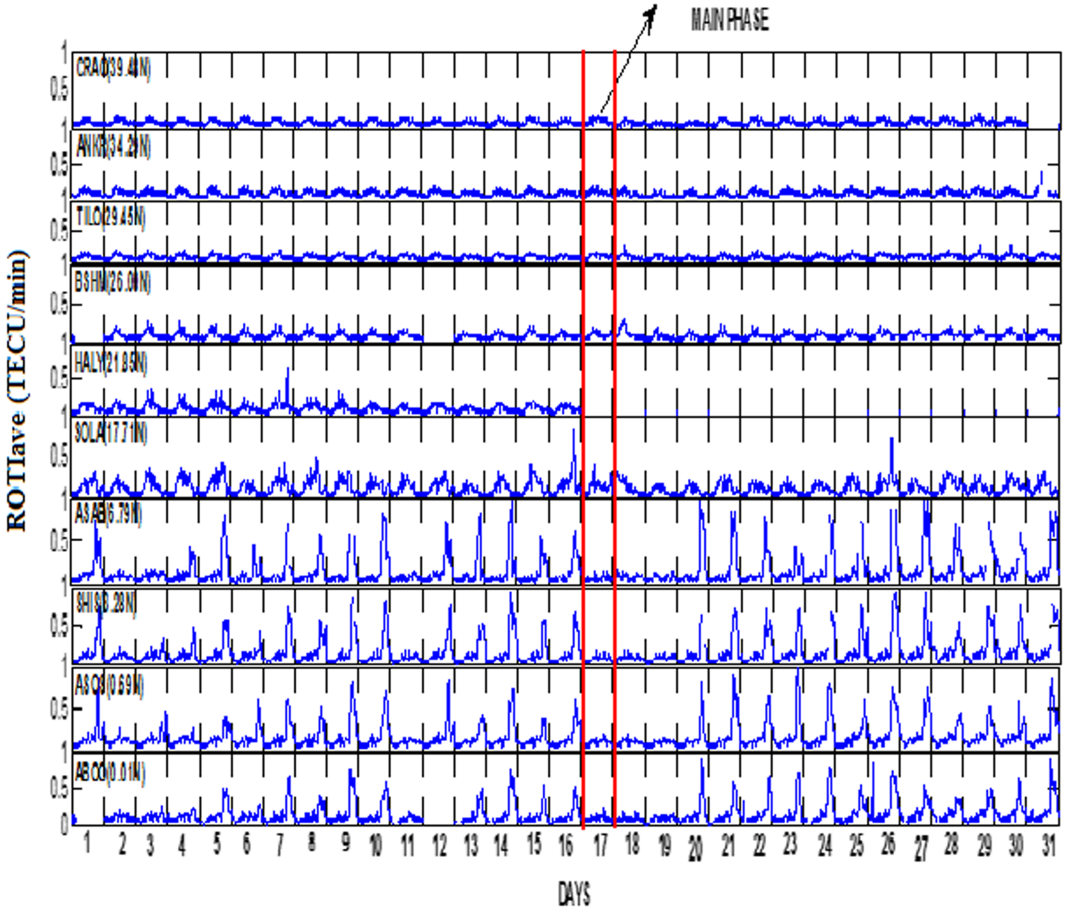

Figure 2. The variation of $ROTI_{ave}$ for stations located in the Northern Hemisphere during the period of 1–31 March 2015.

region. This result is in agreement with the existing knowledge on irregularities. The occurrence is observed to be consistent over the equatorial region for all the days during this period except for storm days.

To investigate the latitudinal distribution of irregularities in the region, the average monthly value of $ROTI_{ave}$ is plotted against magnetic latitudes for each station. The arrangement of the stations is such that they span from the dip equator down to the midlatitude in both hemispheres. The average monthly value of $ROTI_{ave}$ is the average value of $ROTI_{ave}$ for all the quiet days (Kp index ≤ 2) of the month; except at stations where irregularities are observed, it was computed only from quiet days with the presence of irregularities. Figure 4 shows the latitudinal distribution of the monthly average of $ROTI_{ave}$ value between 16:00 and 03:00 LT for the entire stations. From the plots, it can be observed that the appearance of irregularities strongly depends on local time and latitude. Irregularities occurred mostly between 19:00 and 00:00 LT regardless of the hemisphere. This result is also in agreement with previous investigations involving individual location in the region (e.g., Mungufeni et al., 2016). Furthermore, the appearance of irregularity is observed to be earlier in the south, though with a less severity mainly at a station outside the dip equator but close to the equatorward boundary of the EA region. The peak appearance is observed at 21:00 LT, as it is seen across the entire latitudes except for stations outside the equatorial region and it disappeared finally at 01:00 LT. Beyond the ~18° magnetic latitude, it is rarely observed in the south; however, only the background irregularity levels were observed at ~18°N magnetic latitude in the north contrary to the observation in the Southern Hemisphere. This indicates a major asymmetry in terms of the latitudinal boundary between the Northern and Southern Hemispheres. The appearance of irregularities observed in this study during the evening period is in agreement with the existing theory. It well known that the appearance of ionospheric irregularities at the equatorial region has been linked to the lifting of the equatorial F region plasma just

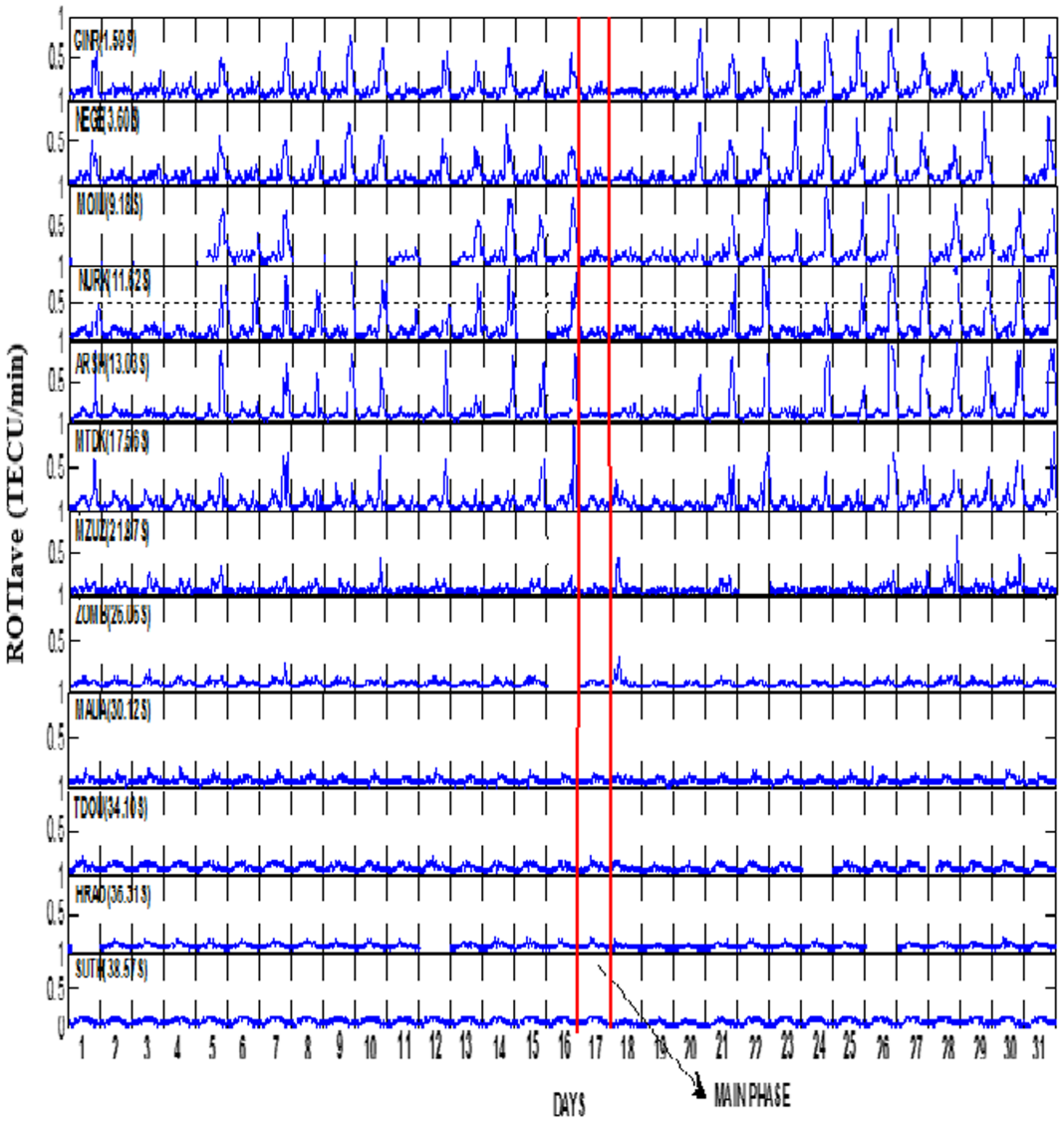

Figure 3. The variation of $ROTI_{ave}$ for stations located in the Southern Hemisphere during the period of 1–31 March 2015.

after sunset and the plasma density decay that occurred at the bottomside ionosphere due to absence of solar ionizing radiation around the same time. The decay in plasma gives rise to steep density gradient and may result to plasma instability at the bottomside. Plasma density perturbation at the bottomside ionosphere can be triggered by the R-T instability. The initial perturbation can however be provided by upward propagating gravity wave (Kelley, 1989).

Furthermore, the strength of irregularities is generally most severe at ~12° magnetic latitude in the south with a peak value of about 1.1 TECU/min observed at 22:00 LT. However, it was observed around ~7°N in the north in most of the hours. The observation in the north may require further investigation because of the wide gap between latitudes ~7° and ~18° in the north due to the absence of GPS receivers. The occurrence of severe irregularity near the anomaly crest region in the south may be an indication that the conditions necessary for occurrence of strong irregularities are most favorable at that region. Such conditions may include higher altitude of the *F* region peak or/and steep background plasma density gradient at the bottomside of the *F* region. Higher altitudes of the *F*2 region due to the evening prereversal plasma drift may be one of the key factors that favor the generation of irregularities. At higher altitude of the *F* region peak, recombination rate is low due low ion-neutral collision frequency; hence, the ambient plasma density at the

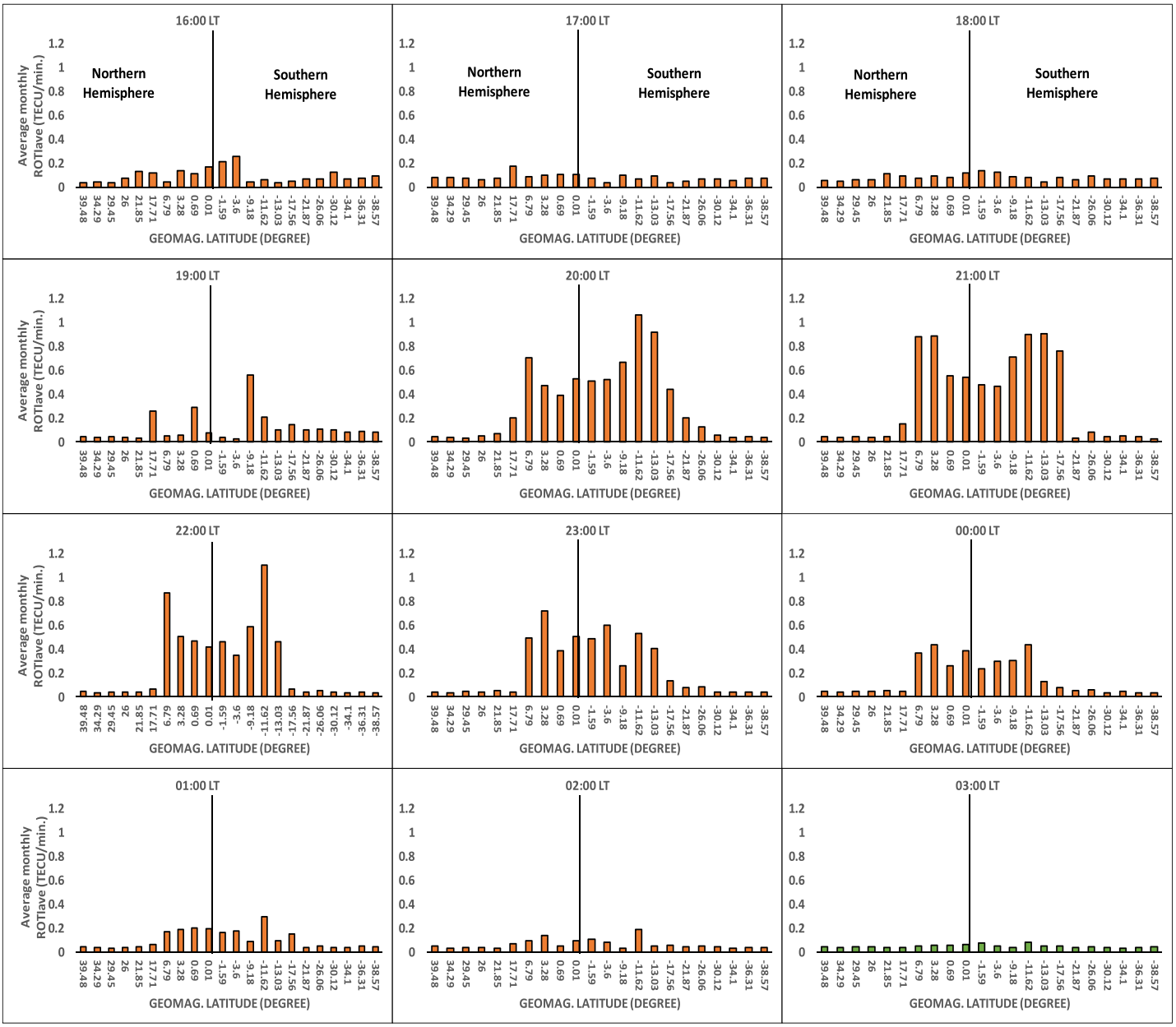

Figure 4. The quiet time latitudinal variation of the average monthly value $ROTI_{ave}$. The plots indicate the average $ROTI_{ave}$ as a function of magnetic latitude for the period 16:00–03:00 LT. The average monthly value of $ROTI_{ave}$ is the average value of ROTIave for all the quiet days (*Kp* index ≤2) of the month, except at stations where irregularities are observed, the average monthly value $ROTI_{ave}$ is computed only from quiet days with the presence of irregularities.

topside *F* region is high. On the other hand, the absence of irregularities at station beyond ±18° may also suggest the absence of either the above factors or the seeding mechanisms necessary for the generations of irregularities at those locations.

3.2. The Effect of 17 March 2015 Storm on the Latitudinal Distribution of Irregularities

Figure 5 shows the variation of geomagnetic indices and interplanetary magnetic field (IMF) parameters against the universal time (UT) from 10 to 31 March, 2015. The parameters include the B_Y and B_Z components of IMF, the solar wind temperature (T), the plasma flow speed (v), the proton density (N_e), the 1-min symmetric H-component (*SYM-H*) and the asymmetric H-component (*ASYM-H*), the average daily planetary *A* index (A_P index), and weighted average 3-hourly planetary *K* index (K_P index).

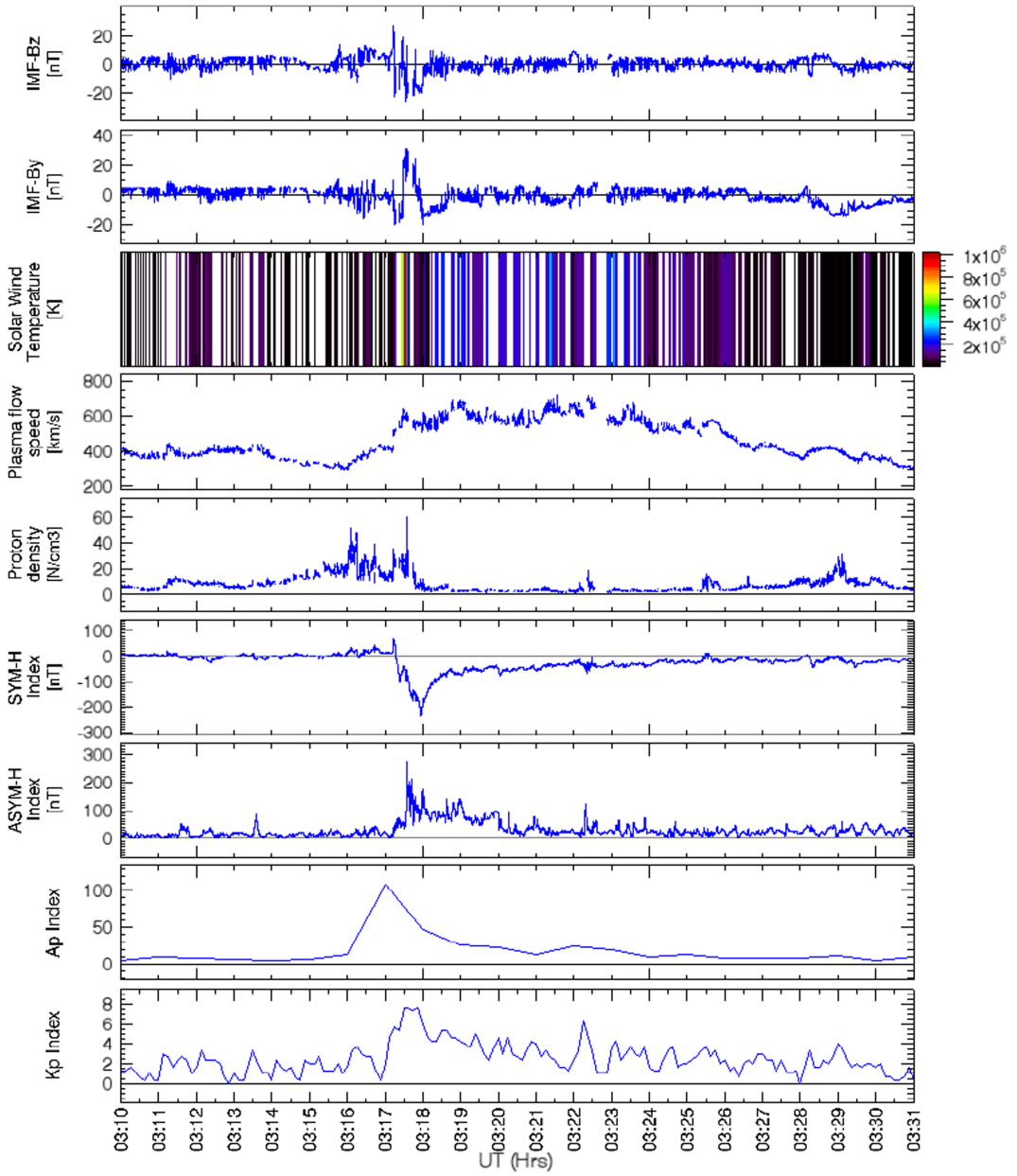

Figure 5. The time variations of IMF parameters and geomagnetic indices for the period of 10–31 March 2015.

Previous investigations have reported that the 17 March 2015 storm event was initiated by the impact of the coronal mass ejections produced by C9 solar flare on the Earth's magnetosphere (Borries et al., 2016; Kataoka et al., 2015). The impact led to increase in most of the IMF parameters (e.g., V_z increases from 400–500 km/s, IMF-B_Z fluctuates from 5 up to 25 nT, etc.) and at the equatorial region; its effect is seen by the rapid increase in the magnitude of *SYM-H* index (up to maximum value of ~70 nT) around 05:00–06:00 UT on 17 March 2015. Also, judging from the *SYM-H* index variation (which indicates the dynamics of the ring current) shown in Figure 5, this storm event can be classified as very intense storm (minimum value of *SYM-H* index is −234 nT) with a double-step main phase and a recovery phase that lasted for several days. The first step of the negative excursion of *SYM-H* is observed between 06:00 and 09:30 UT on 17 March 2015 following the abrupt southward incursion of IMF-B_Z from its northward path. This is followed by a partial recovery that lasted for about 3 hr on the same day, and this corresponds to the period when the IMF-B_Z turned northward from southward orientation. The second step of the main

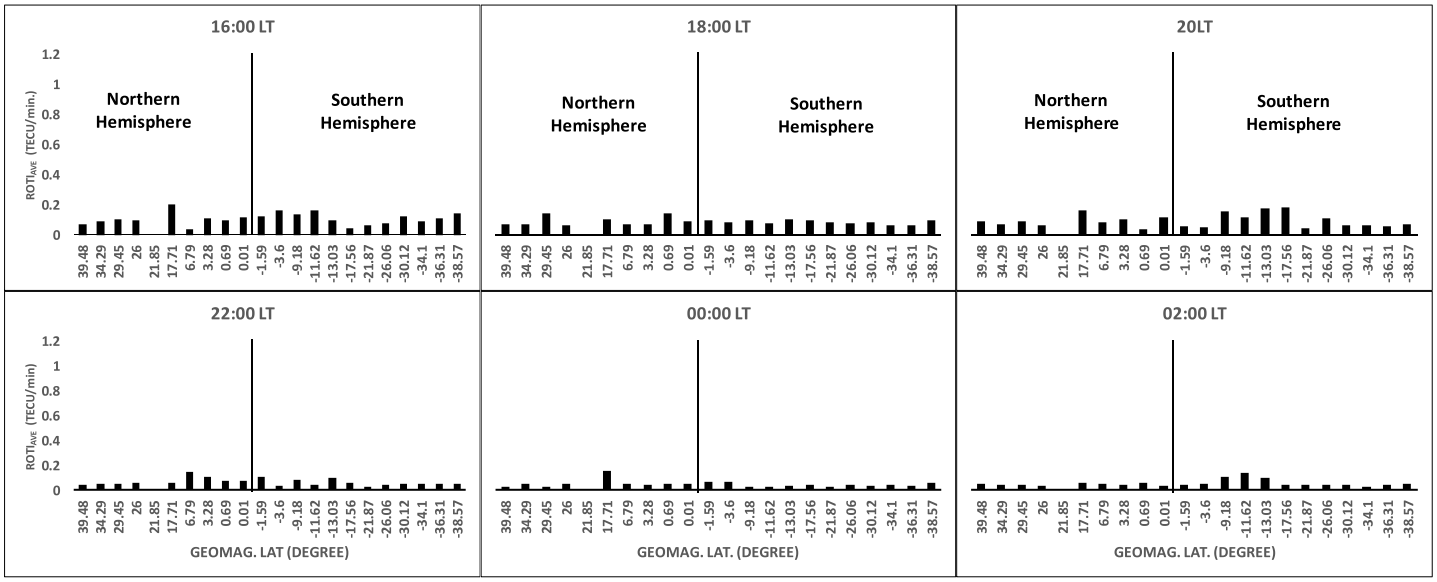

Figure 6. The latitudinal variation of ROTI$_{ave}$ on the night following the main phase. The plots indicate ROTI$_{ave}$ value as a function of magnetic latitude for the period 16:00–02:00 LT on 17 March 2015.

phase occurred between 12:00 and 23:00 UT on the same day, and this is when *SYM-H* reached its minimum value. This interval also corresponds to the time when the orientation of B_Z is southward, and it remains there for a long duration that lasted for about 11hr. The recovery phase started immediately after the peak minimum value of *SYM-H* is reached and lasted for several days before full recovery condition is attained.

As indicated in Figures 2 and 3, the absence of spike between 17 and 20 March 2015, particularly at the equatorial stations, suggests that there are no irregularities during those periods. To further investigate this, the latitudinal distribution during the main phase and night of the first recovery days is analyzed and the results are presented in Figures 6 and 7, respectively. Each panel in the two figures represents the hourly ROTI$_{ave}$

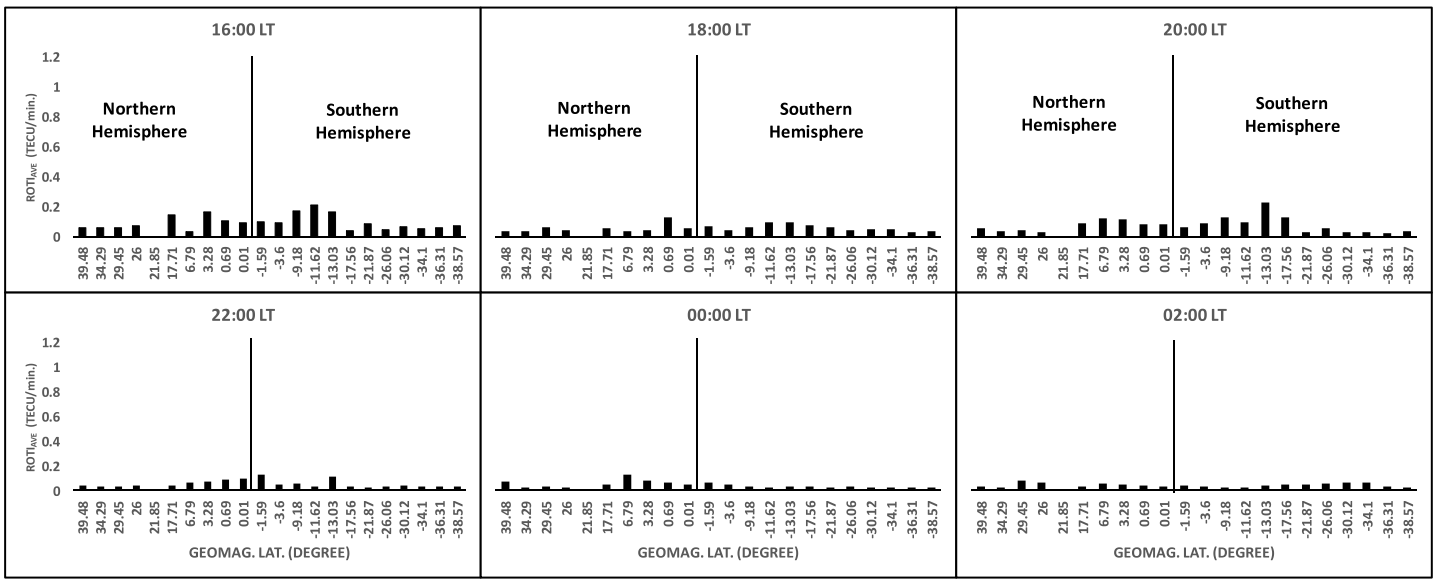

Figure 7. The latitudinal variation of ROTI$_{ave}$ on the night following the first day of recovery phase. The plots indicate ROTI$_{ave}$ as a function of magnetic latitude for the period 16:00–02:00 LT on 18 March 2015.

value in all the stations. As indicated in the two figures, the results obtained confirm the absence of irregularities across the entire latitudes on the night of the two disturbed days considered. This result is in agreement with the result of Bolaji et al. (2019) over the region. Just recently, Bolaji et al. (2019) investigated the effect the same storm event had on the longitudinal distribution of ionospheric irregularities. Their result showed a considerable longitudinal difference in the occurrence of irregularities during the night following the main phase and first day of recovery phase.

The absence of irregularities during the storm days may be due to the suppressive action of the storm event on drivers that may trigger its development. The main phase of the storm event considered occurred around the local sunrise and persisted until the midnight periods. This period corresponds to when the undershielding electric fields penetrate through the entire latitudes and its polarity at low-latitude region may impede or enhance the development of irregularities. The absence of irregularities observed during the night following the main phase may suggest that the electric fields injected into the region during the main phase may have inhibited the initiation of R-T processes and hence may prevent the development of irregularities on that day. Furthermore, the result observed during the first night of the storm recovery also indicates the absence of irregularities. This may be attributed to the mechanical effect of storm-induced drivers such as the effect of disturbance dynamo electric fields. It is well known that the Joule heating of the polar region during geomagnetic storm due precipitation of high energetic particle into the region sets up a pressure gradient that may cause a significant perturbation in the global thermospheric wind systems. At the equatorial region, such perturbation in the thermospheric wind may generate disturbance dynamo electric fields, whose polarity is such that may favor or impede the development of irregularities. The polarity of electric fields which favors the generation of irregularities is such that it is eastward during daytime. Daytime imposition of westward electric field due to storm activity may counterbalance the usual eastward fields and hence may impede those mechanisms that may favor the generation of irregularities (e.g., the evening vertical upward drift and *hmF*2 increase) as observed in this case.

4. Conclusion

This paper has investigated the latitudinal distribution of irregularities over the African ionosphere in March 2015. This period of study included days that are considered to be magnetically quiet and also extremely disturbed. The results obtained lead to the following conclusions:

1. The appearance irregularities are mostly observed between 19:00 and 00:00 LT in the region during the period considered.
2. Its appearance is earlier at the Southern Hemisphere toward the equatorward edge of the EIA.
3. The peak of its occurrence is at 21:00 LT. The occurrence at this time is found to be most severe and is seen over the entire latitudes except those outside the equatorial region.
4. The maximum severity occurred around the ∼12° geomagnetic latitude in the south during the period considered with a value up to 1.10 TECU/min. The exact location in north cannot be determined due to data gap.
5. Irregularity is found up to around ∼18° geomagnetic latitude in the south; beyond this latitude it is rarely noticed. However, it is not seen up to ∼18°N contrary to the observation at Southern Hemisphere. This shows a major hemispheric asymmetry in terms of latitudinal boundary.
6. Its disappearance is faster around the poleward verge of the EIA particularly in the south.
7. Lastly, it was found that the 17 March 2015 storm event hindered the appearance of irregularities across the entire latitudes in the region during the nights of the main phase and the one following the first day of recovery phase.

Acknowledgments
The African Geodetic Reference Frame (http://www.afrefdata.org) and International GNSS Service (ftp://garner.ucsd.edu/rinex) where the GPS data are obtained are acknowledged. We thank the NASA Goddard Space Flight Center, Space Physics data facility (https://omniweb.gsfc.nasa.gov/form/dx1.html) for the interplanetary magnetic field (IMF) data and the World Data Center for geomagnetism, Kyoto University, Japan, for the geomagnetic indices (wdc.kugi.kyoto-u.ac.jp). The authors also appreciate Gopi Krishna Seemala of the Indian Institute of Geomagnetism for the GPS-TEC analysis software.

References

Amaechi, P. O., Oyeyemi, E. O., & Akala, A. O. (2018). Geomagnetic storm effects on the occurrences of ionospheric irregularities over the African equatorial/low-latitude region. *Advances in Space Research*, *2018*. https://doi.org/10.1016/j.asr.2018.01.035

Anderson, D., Anghel, A., Chau, J., & Veliz, O. (2004). Daytime vertical E_B drift velocities inferred from ground-based magnetometer observations at low latitudes. *Space Weather*, *2*, S11001. https://doi.org/10.1029/2004SW000095

Bolaji, O. S., Adebiyi, S. J., & Fashae, J. B. (2019). Characterization of ionospheric irregularities at different longitudes during quiet and disturbed geomagnetic conditions. *Journal of Atmospheric and Solar-Terrestrial Physics*, *182*, 93–100.

Borries, C., Mahrous, A. M., Ellahouny, N. M., & Badeke, R. (2016). Multiple ionospheric perturbations during the Saint Patrick's day storm 2015 in the European-African sector. *Journal of Geophysical Research, Space Physics*, *121*(11), 11,333–11,345. https://doi.org/10.1002/2016JA023178

De Rezende, L. F. C., De Paula, E. R., Batista, I. S., Kantor, I. J., & De Assis Honorato Muella, M. T. (2007). Study of ionospheric irregularities during intense magnetic storms. *Brazilian Journal of Geophysics*, *25*, 151–158.

Deng, B., Huang, J., Kong, D., Xu, J., Wan, D., & Lin, G. (2014). Temporal and spatial distributions of TEC depletions with scintillations and ROTI over south China. *Advances in Space Research*, *55*(1), 259–268.

Dugassa, T., Habarulema, J. B., & Nigussie, M. (2019). Longitudinal variability of occurrence of ionospheric irregularities over the American, African and Indian regions during geomagnetic storms. *Advances in Space Research*. https://doi.org/10.1016/j.asr.2019.01.001

Fejer, B. G., Scherliess, L., & de Paula, E. R. (1999). Effects of the vertical plasma drift velocity on the generation and evolution of equatorial spread F. *Journal of Geophysical Research*, *104*(A9), 19,859–19,869.

Kataoka, R., Shiota, D., Kilpua, E., & Keika, K. (2015). Pileup accident hypothesis of magnetic storm on 17 March 2015. *Geophysical Research Letters*, *42*, 5155–5161. https://doi.org/10.1002/2015GL064816

Kelley, M. C. (1989). *Ionospheric radio*. London: Peter Peregrinus Ltd.

Kil, H., Paxton, L. J., & Oh, S.-J. (2009). Global bubble distribution seen from ROCSAT-1 and its association with the evening pre-reversal enhancement. *Journal of Geophysical Research*, *114*, A06307. https://doi.org/10.1029/2008JA013672

Kintner, P., T. Humphreys, and J. Hinks (2009), GNSS and ionospheric scintillation: How to survive the next solar maximum? Inside GNSS, July/August, 22–30. [Available at www.insidegnss.com.]

Kintner, P. M., Ledvina, B. M., & de Paula, E. R. (2007). GPS and ionospheric scintillations. *Space Weather*, *5*, S09003. https://doi.org/10.1029/2006SW000260

Lee, C. C., Chu, F. D., Chen, W. S., Liu, J. Y., Su, S. Y., Liou, Y. A., & Yu, S. B. (2009). Spread F, GPS phase fluctuations, and plasma bubbles near the crest of equatorial ionization anomaly during solar maximum. *Journal of Geophysical Research*, *114*, A08302. https://doi.org/10.1029/2009JA014195

Li, G., Ning, B., Hu, L., Liu, L., Yue, X., Wan, W., et al. (2010). Longitudinal development of low-latitude ionospheric irregularities during the geomagnetic storms of July 2004. *Journal of Geophysical Research*, *115*, A04304. https://doi.org/10.1029/2009JA014830

Li, G., Ning, B., Liu, L., Zhao, B., Yue, X., Su, S.-Y., & Venkatraman, S. (2008). Correlative study of plasma bubbles, evening equatorial ionization anomaly, and equatorial pre-reversal EXB drifts at solar maximum. *Radio Science*, *43*, RS4005. https://doi.org/10.1029/2007RS003760

Li, G., Ning, B., & Yuan, H. (2007). Analysis of ionospheric scintillation spectra and TEC in the Chinese low latitude region. *Earth, Planets and Space*, *59*, 279–285.

Mendillo, M., Lin, B., & Aarons, J. (2000). The application of GPS observations to equatorial aeronomy. *Radio Science*, *35*(3), 885–904.

Muella, M. T. A. H., de Paula, E. R., Kantor, I. J., Batista, I. S., Sobral, J. H. A., Abdu, M. A., et al. (2008). GPS L-band scintillations and ionospheric irregularity zonal drifts inferred at equatorial and low-latitude regions. *Journal of Atmospheric and Solar-Terrestrial Physics*, *70*, 1261–1272.

Mungufeni, P., Habarulema, J. B., & Jurua, E. (2016). Trends of ionospheric irregularities over African low latitude region during quiet geomagnetic conditions. *Journal of Atmospheric and Solar-Terrestrial Physics*, *138-139*, 261–267.

Ngwira, C. M., Seemala, G. K., & Habarulema, J. B. (2013). Simultaneous observations of ionospheric irregularities in the African low-latitude region. *Journal of Atmospheric and Solar-Terrestrial Physics*, *97*, 50–57.

Oladipo, O. A., & Schüler, T. (2013a). Equatorial ionospheric irregularities using GPS TEC derived index. *Journal of Atmospheric and Solar-Terrestrial Physics*, *92*, 78–82.

Oladipo, O. A., & Schüler, T. (2013b). Magnetic storm effect on the occurrence of ionospheric irregularities on an equatorial station in the African sector. *Annals of Geophysics*, *56*(5), A0565.

Olwendo, O. J., Baluku, T., Baki, P., Cilliers, P. J., Mito, C., & Doherty, P. (2013). Lowlatitude ionospheric scintillation and zonal irregularity drifts observed with GPS- SCINDA system and closely spaced VHF receivers in Kenya. *Advances in Space Research*, *51*, 715–1726.

Pi, X., Mannucci, A. J., Lindqwister, U. J., & Ho, C. M. (1997). Monitoring of global ionospheric irregularities using the world wide GPS network. *Geophysical Research Letters*, *24*(18), 2283–2286.

Wiens, R. H., Ledvina, B. M., Kintner, P. M., Afewerki, M., & Mulugheta, Z. (2006). Equatorial plasma bubbles in the ionosphere over Eritrea: Occurrence and drift speed. *Annales de Geophysique*, *24*, 1443–1453.